IMEKO 2010 TC3, TC5 and TC22 Conferences
Metrology in Modern Context
November 22–25, 2010, Pattaya, Chonburi, Thailand

OPTIMUM DIMENSIONS OF DWM LOADING FRAME

A. Abu-Sinna [1], *Yon-Kyu Park* [2], *Dae-Im Kang* [2], *Min-Seok Kim* [2]

[1]Force and Material Metrology Department (FMMD), National Institute for Standards (NIS), Giza, Egypt, a.abu.sinna@nis.sci.eg
[2] Division of Physical Metrology, Korea Research Institute of Standards and Science (KRISS), Daejeon, Republic of Korea, ykpark@kriss.re.kr, dikang@kriss.re.kr

Abstract – In this paper, we are willing to know the influence of the loading frame stiffness through finite element method. FEM modelling has to be run with different force application criteria, and different dimensions of loading frames. In addition, different dimensions of loading frame have been dedicated to run the experiments.

The upper plate dimensions showed the superiority over all other loading frame components, and consequently the priority of the rigid loading frame. Hence, supplementary measurements as well as FEM modelling were performed to identify the exact influence and generalize the conclusions through different types of loadcells.

An empirical formula (I_X/F) was calculated for comparing different behaviours of loadcells using different models of loading frames. In addition, three types of loadcells were examined for final conclusion.

Keywords: Deadweight Machine, Loading Frame, Loadcell, FEM.

1. INTRODUCTION

Several studies had been established to investigate the interaction between the Dead Weight Machines (DWM) and the loadcells. As a result, the main reasons that propagate the interaction between the DWM and loadcell may be categorized into three main categories; force application, vibrations, and environmental conditions. Bray *et al.* [1, 2] and Kovacs S. [3] have investigated the force application. They analyzed the force application into application time, force centring, differences in physical characteristics between the loadcell pad and cap, stiffness of loadcells and DWM structures, and parasitic effects. Robinson [4, 5] investigated the effect of force centring and the influence of contact stresses during measurements. Ferrero *et al.* [6] showed that a six-component dynamometer provides an accurate method for measuring the parasitic forces and moments, while Park Y. K. and Kang D. I. [7] proposed a new method for estimating the parasitic forces and moments using a build-up system. The presence of vibrations, both transferred through pendulum motion of the masses and measured using a build-up system [8, 9], and those transferred due to vibrations of the machine itself, foundation vibrations, and outer environmental vibrations, [10, 11] have caused much concern. This suggested that the loading frame stiffness is a likely candidate for the cause of the interaction problems.

The primary conclusion of a past work for the authors [12] was that the upper plate thickness is most influential parameter within the four loading frame's dimension variables investigated, which are the upper plate thickness, span width, loading frame height, and column diameter and it consequently demonstrates the importance of a rigid loading frame in DWMs.. Finite element analysis illustrated that the upper plate thickness is the most important of these four factors. In order to perform the finite element analysis efficiently, a utilization of the Taguchi technique was implemented, as this typically reduces the total required simulations. The validity of the finite element analysis was confirmed through experiments.

However, in this paper, in order to determine the exact behaviour of the loadcell output for loading frames with different upper plate thicknesses, and to specify the required thickness for designing DWMs, a series of generalizing simulations were carried out using FEM modelling.

2. FEM SIMULATION

Regarding the establishment of the framework of the investigation, many factors should be discussed and selected and hence the steps of the modelling could be arrayed. First item to be analyzed to its main factors is the loading frame construction, which simply can be classified into; upper plate, lower plate and column, while the second item to be analyzed in the investigation is the loadcell. In the following clauses a description will be introduce to the loading frame models, loadcell models and simulation protocol.

2.1. Design of the models

In the previous investigation [12], the superiority of the upper plate thickness was derived and confirmed using a series of experimental measurements and FEM simulations. In order to carry out the FEM simulation in compatibility with the models of the previous work, different models of loading frames were designed and put into simulation along with three types of loadcells. The loadcells were illustrating three types; column type, beam type, and S-type.

In these simulations, the width of the span cross-sectional area b, was fixed to 10 mm, the diameter of the loading frame columns, d, was fixed to 8 mm, the span

width of the loading frame, L, was fixed to 150 mm and the loading frame height, H, was fixed to 300 mm, where the upper plate thicknesses h, of 4, 8, 10, 12, 14, 16, 18, 20, 22, 24, and 26 mm were investigated. The values of d, L, and H were chosen as a result of the modelling and experiments (in comparison with the upper plate thickness) suggested that there is no significant variation as these parameters changed. The values used for d, L, and H are the average values from the previous models discussed in Section 2 [12]. Figure 1 shows the dimensions of the loading frame.

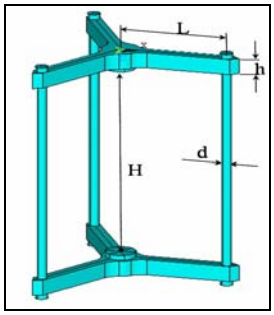

Fig. 1. A schematic diagram indicating the dimensions of the model used in the FEM.

2.2. Simulation protocol

The simulations were run by applying the loads on the loading frame-loadcell model and deducing the behaviour of the model by comparing the results of four practical strain gauges positions distributed all over the loadcell sensing element. The resultant strain in tangential direction was calculated at each node lies on the comparable paths. It was taken to be significant in monitoring the trends between various models. The measuring locations of the strain gauges were set in four positions for the three different loadcells as seen in the Figures 2, 3, and 4. The four strain gauges, SG1, SG2, SG3, and SG4 shall represent the strain gauges used in the real loadcells.

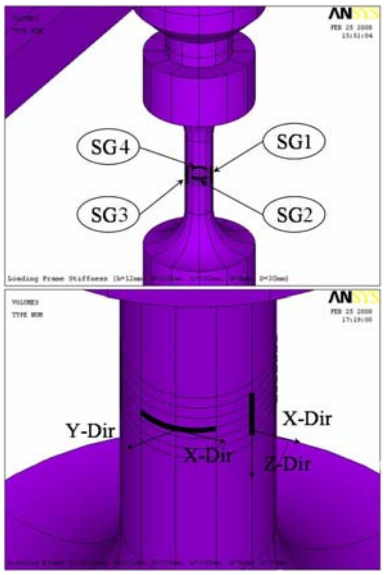

Fig. 2. The positioning of the four strain gauges in the FEM ANSYS, Column-Type loadcell structure.

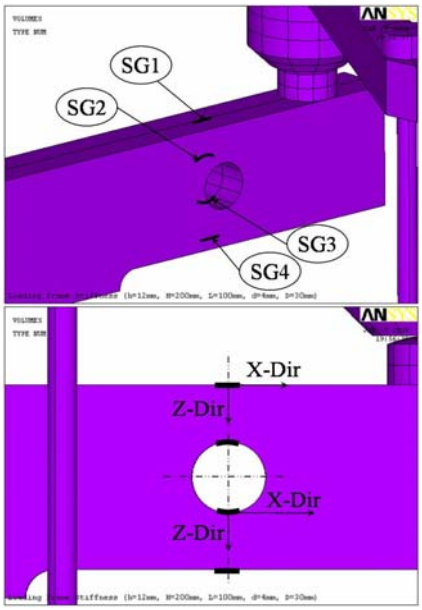

Fig. 3. The positioning of the four strain gauges in the FEM ANSYS, Beam-Type loadcell structure.

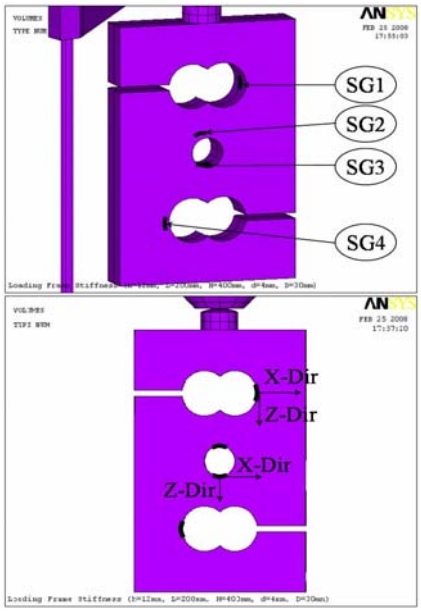

Fig. 4. The positioning of the four strain gauges in the FEM ANSYS, S-Type loadcell structure.

The characteristics of the four strain gauges are, 3 mm length, and 13 Nodes in the designed meshing system. The calculations of the results were based on the resultant tangential XZ-strain for each node, in case of SG1, SG2, SG3, and SG4 in both Beam-Type model and S-Type model, and case of SG1 and SG3 in Column-Type model. While in case of SG2 and SG4 in Column-Type model the calculations of the results based on the resultant tangential XY-Strain for each node, Figures 5, 6, and 7. Where, the average of the 13 nodes XZ-Strain has been calculated and hence each model can produce four strains representing four strain gauges locations. The FEM simulation is based on the equations (1) and (2).

$$SG_j = \sum_{i=1}^{i=n} \delta_{iTan} \tag{1}$$

$$SG_T = \sum_{j=1}^{j=m} \left| SG_j \right| \tag{2}$$

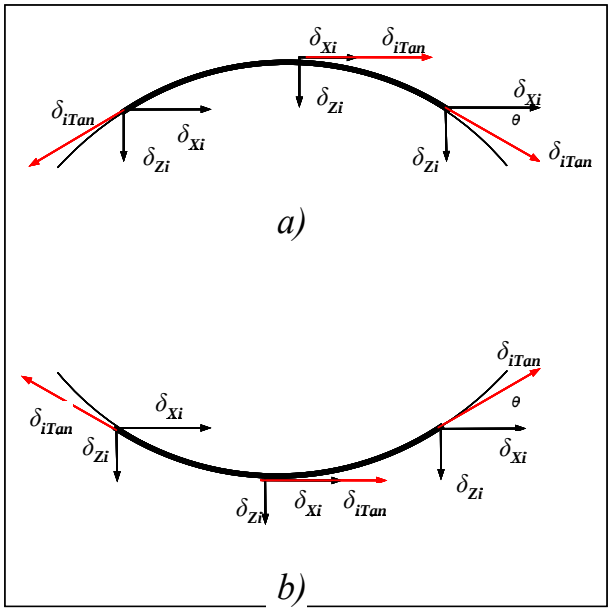

Fig. 5. A schematic drawing representing the tangential strain as a resultant strain in X and Z directions. a) Is a representation of Path No. 2 in both Beam-Type Loadcell and S-Type loadcell (SG2). b) Is a representation of Path No. 3 in both Beam-Type Loadcell and S-Type loadcell (SG3).

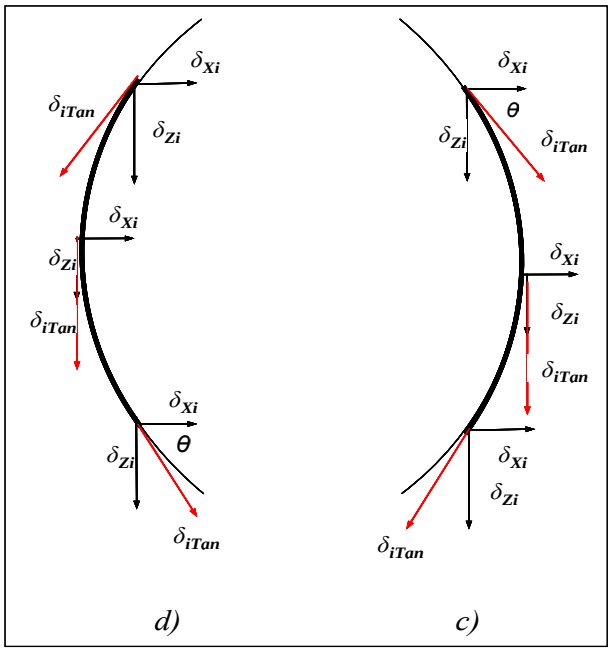

Fig. 6. A schematic drawing representing the tangential strain as a resultant strain in X and Z directions. c) Is a representation of Path No. 1 in S-Type loadcell (SG1). d) Is a representation of Path No. 4 in S-Type loadcell (SG4).

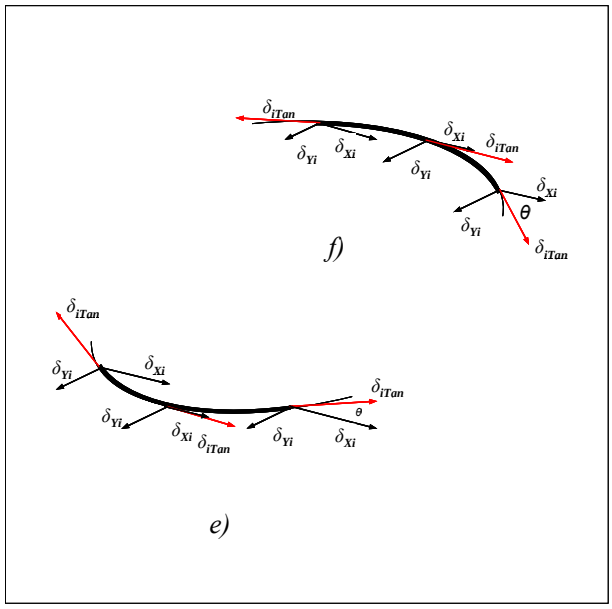

Fig. 7. A schematic drawing representing the tangential strain as a resultant strain in X and Y directions. e) Is a representation of Path No. 2 in Column-Type loadcell (SG2). f) Is a representation of Path No. 4 in Column-Type loadcell (SG4).

Knowing that:
for the Beam-Type Loadcell (Paths 1 and 4)

$$\delta_{iTan} = \delta_{Xi} \tag{3}$$

for the Beam-Type Loadcell (Paths 2 and 3)

$$\delta_{iTan} = \delta_{Xi} Cos\theta + \delta_{Zi} Sin\theta \tag{4}$$

for the Column-Type Loadcell (Paths 1 and 3)

$$\delta_{iTan} = \delta_{Zi} \tag{5}$$

for the Column-Type Loadcell (Paths 2 and 4)

$$\delta_{iTan} = \delta_{Xi} Cos\theta + \delta_{Yi} Sin\theta \tag{6}$$

for the S-Type Loadcell (Paths 1 and 4)

$$\delta_{iTan} = \delta_{Xi} Sin\theta + \delta_{Zi} Cos\theta \tag{7}$$

for the S-Type Loadcell (Paths 2 and 3)

$$\delta_{iTan} = \delta_{Xi} Cos\theta + \delta_{Zi} Sin\theta \tag{8}$$

Where:

SG_T	is the total strain value per model.
SG_j	is the summation of strain values per each path.
δ_{iX}	is the Strain value at each node in X-Direction.
δ_{iY}	is the Strain value at each node in Y-Direction.
δ_{iZ}	is the Strain value at each node in Z-Direction.
δ_{iTan}	is the Tangential Strain value calculated (XZ-Dir. or XY-Dir.).
n	no. of nodes per each strain gauge (=13).
m	no. of strain gauges per loadcell (=4).

The output of the different FEM simulations (132 models) is essentially the resultant tangential strain, in XZ

direction in some cases and XY directions in other cases as mentioned before. Therefore, after calculating the tangential strain at each node (13 nodes per each strain gauge path), the accumulation of the four paths (SG1, SG2, SG3, and SG4) took place and hence the simulation output introduced. In case of ideal loading, only one loading condition was applied without rotations, since the output, in other positions, will be the same, while three rotations, 0^O, 120^O, and 240^O, were examined in case of 1^O inclination. These steps have been repeated for all three types of loadcells used.

2.3. Calculations

Ferrero *et al.* [13] stated that the observed values of the side force and bending moments correspond respectively, to a maximal inclination of 10^{-3} rad, and to an eccentricity of 10^{-4} m of the load application line to the axis of the dynamometer for the standard dead weight machine considered. Among his conclusions, he stated that, the side components depend mainly on the initial machine inclination and on a possible rotation of the adjustable crossbeam. In order to observe and track the effect of these effects clearly, the inclination angle chosen to equal 1^O.

In the FEM simulation, the force adaptation was made during the construction of the models by slightly rotation of the axis of the loadcell model under process by an angle equal to 1^O as seen in Figure 8.

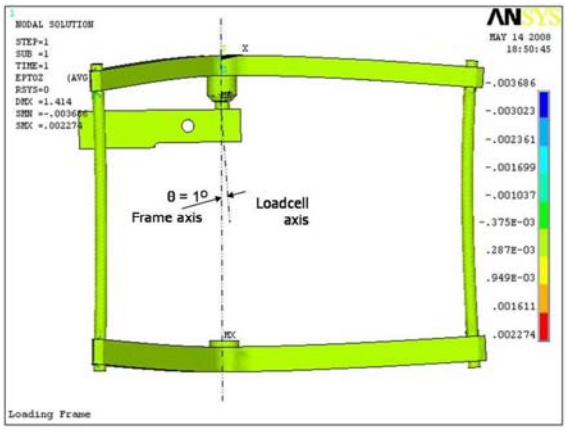

Fig. 8. A schematic drawing for the inclination angle 1^O for force adaptation in the FEM simulation.

The term of relative deviation was considered as a comparable value between the experiments in a way to eliminate and minimize any interaction due to rotational effect. Next equation identifies the value of the relative deviation.

$$Rel.Dev. = \frac{SG_{T_I} - SG_{T_O}}{SG_{T_O}} \quad (9)$$

Where:

SG_{TI} is the average of three positions (0^O, 120^O, 240^O) with inclination angle 1^O.

SG_{To} is the output without inclination angle (Ideal, 0^O).

One more additional hypothesis, that to make comparison between different upper plate thicknesses, which assumed up till now has a rectangular cross sectional area, we are in need to insert the value of the cross section area in the comparison process. Such assumption will facilitate the comparisons even between different shapes of upper plate cross sections. Therefore, the calculations will base on the using of the second moment of inertia of the upper plate thickness with respect to the generated force. This relative term can be expressed in I_X/F (mm^4/N), where I_X is the second moment of inertia and F is indicating the generated force. By applying the rated force equal to 200 N, this will set the relative term (I_X/F) to equal 0.27, 2.13, 4.17, 7.2, 11.43, 17.07, 24.3, 33.33, 44.36, 57.6, and 73.23 mm^4/N respectively.

3. RESULTS

As mentioned before, the column type, the beam type, and the S-type loadcells were chosen to be the models used in the present simulation. In addition, the same circumferential loading cases used in clause 2.2 were repeated. The results of these 11 verification modelling were graphed in Figures 9, 10, and 11.

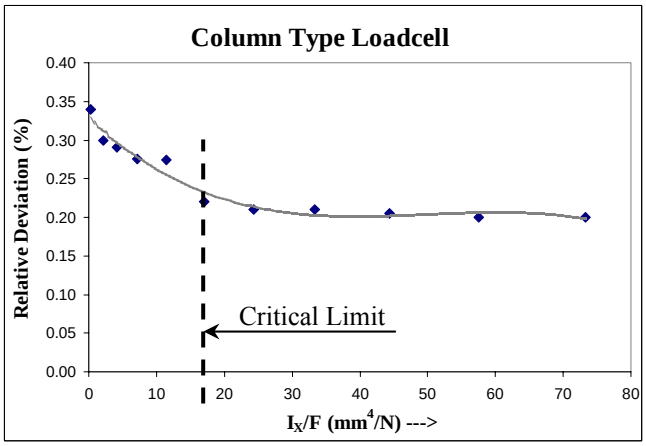

Fig. 9. Relationship between the relative deviation and the upper plate thickness for the column type loadcells.

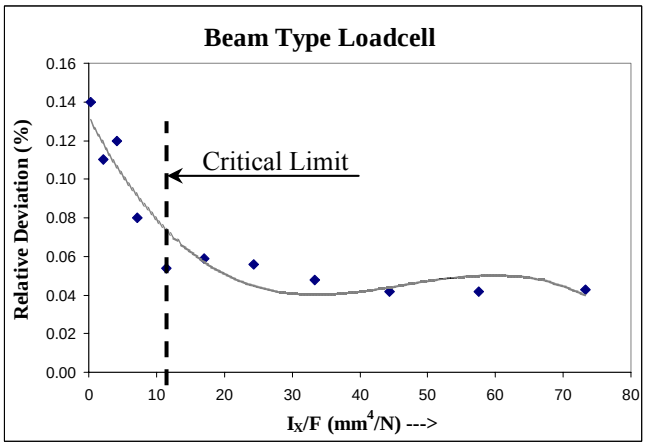

Fig. 10. Relationship between the relative deviation and the upper plate thickness for the beam type loadcells.

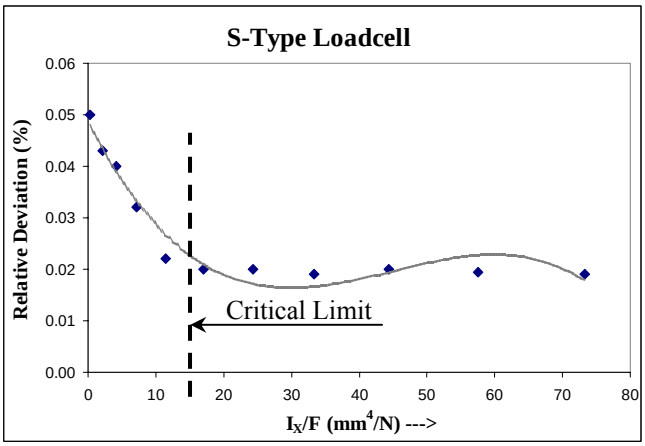

Fig. 11. Relationship between the relative deviation and the upper plate thickness for the s-type loadcells.

In figure 9, the inverse relationship is very clear, especially for I_X/F is < 18 mm^4/N. This value (18 mm^4/N) can be considered as a border for the critical limits. Simply we can see that the behaviour of the relation is completely different prior and following this value. While the slope of the trend line is obviously sharp, prior the critical limit (18 mm^4/N), it showed a much more steady state and tends to be constant after the critical limit.

The observation noticed in the column type loadcell repeated itself in the other two types, beam and S. In figure 10, for the relationship between the relative deviation and I_X/F, the same behavior was re-performed and the inverse relationship is very clear, especially for I_X/F is < 12 mm^4/N. while the slope of the trend line is obviously sharp, prior the critical limit (12 mm^4/N), it showed a much more steady state and tends to be constant after the critical limit. Synchronously, the S-type loadcell, figure 11, showed the same attitude like column and beam types. The critical limit for the S-type was estimated to be < 15 mm^4/N.

It can be conclude from Figures 9, 10, and 11 that the larger the second moment of inertia (hence the greater the upper plate thickness), the better the lower the relative deviations. It is clear that the difference in magnitude of the relative deviations stops decreasing when I_X/F exceeds 18, 12, and 15 mm^4/N, for column, beam, and S-types respectively, and can be ignored in comparison with differences observed when I_X/F > 18, 12, 15 mm^4/N respectively. However, and as a generalization role, it is preferred for all DWM designers to consider the value of I_X/F to be equal to or better than 20 mm^4/N.

4. CONCLUSIONS

In the way of plotting accurate guidelines for the manufacturers of the DWMs, this investigation was ran and the primary results was published [12]. In the previous work the superiority of the upper plate thickness was confirmed, however results in the present paper are assuring the importance of the rigid loading frames.

A comparison between 132 different loading frame models is suggesting that the second moment of inertia (of the upper plate) must rise to a value that meet the condition I_X/F > 18, 12, 15 mm^4/N for the column, beam ,and S-type loadcells respectively. Since the types of loadcells exceed these representatives, an estimation of $I_X/F \geq 20$ mm^4/N is a secured limit.

For activating more research in DWM-Loadcell interaction, another investigation that suggest another way of focusing on the stiffness of the loading frame construction rather than modification of dimensions, e.g. different materials for both loading frame and loadcell.

ACKNOWLEDGMENTS

The author is grateful to the force group members for their effective cooperation and encouragement.

5. REFERENCES

[1] A. Bray, C. Ferrero, R. Levi, C. Marinari, "An investigation on parasitic effects on force standard machines", *VDI-Berichte,* 312, 113–123, 1978.

[2] S. Kovacs, "Effects of eccentrically and non-axial loads upon the sensitivity of strain gauge load cells", *VDI-Berichte*, 176, 73-91, 1972.

[3] A. Bray, G. Barbato, R. Levi, *Theory and Practice of Force Measurement*, Academic Press, London, 1990.

[4] G. M. Robinson, "Errors due to axisymmetric non-uniform loading of column loadcells", *Measurement*, vol. 7 (1), 30-34, 1987.

[5] G. M. Robinson, "The influence of contact stresses on cylindrical strain gauge load cells", *XIV IMEKO TC-3 Conference*, pp. 129–134, Warszawa, Poland, Sept. 1995.

[6] C. Ferrero, C. Marinari, E. Martino, "A six-component dynamometer to measure parasitic load components on deadweight force standard machines", *X IMEKO TC-3 Conference*, pp. 199-204, Kobe, Japan, Sept. 1984.

[7] Y.K. Park, M.S. Kim, J.H. Kim, D.I. Kang, "A proposal for an evaluation method of force standard machines by using build-up system", *XIX IMEKO TC-3 Conference*, Cairo, Egypt, Feb. 2005.

[8] Y.K. Park, D.I. Kang, "Oscillating signal components of a deadweight force-standard machine and reduction technique", *Meas. Sci. Technol*, vol. 10, pp. 748-754, 1999.

[9] Y.K. Park, D.I. Kang, R. Kumme, A. Sawla, "Investigation of the dynamic behavior of PTB deadweight force standard machines", *XVII IMEKO TC-3 Conference*, pp. 28-35 Istanbul, Turkey, Sept. 2001.

[10] E. Bilgic, B. Karaboce, E. Sadikoglu, S. Fank, "Influence of mechanical vibration on strain gage based force transducer performance", *XVII IMEKO TC-3 Conference*, pp. 195-200 Istanbul, Turkey, Sept. 2001.

[11] M. Nakatani, K. Kameoka, G. Komatsu, N. Inui, K. Naito, H. Konishi, Y. Shimomae, "Effect of floor vibration on a double-beam type loadcell scale", *XVI IMEKO TC-3 Conference*, pp. 460-467, Taejeon, S. Korea, 1998.

[12] A. Abu-Sinna, Yon-Kyu Park, Dae-Im Kang, Min-Seok Kim, "The influence of loading frame stiffness on loadcell-deadweight force machine interaction", *Measurement*, vol. 42, pp. 830-835, 2009.

[13] C. Ferrero, C. Marinari, E. Martino, "The measurement of parasitic components to improve national force standards", *XI IMEKO TC-3 Conference*, pp. 191-208, Houston, Texas, USA, 1988.